7636–7650 *Nucleic Acids Research, 2007, Vol. 35, No. 22* *Published online 2 November 2007*
doi:10.1093/nar/gkm931

Regulatory mechanisms for 3′-end alternative splicing and polyadenylation of the Glial Fibrillary Acidic Protein, GFAP, transcript

Jenny Blechingberg[1], Søren Lykke-Andersen[2], Torben Heick Jensen[2], Arne Lund Jørgensen[1] and Anders Lade Nielsen[1,*]

[1]Institute of Human Genetics, The Bartholin Building and [2]Centre for mRNP Biogenesis and Metabolism, Department of Molecular Biology, University of Aarhus, DK-8000 Aarhus C, Denmark

Received August 28, 2007; Revised October 10, 2007; Accepted October 11, 2007

ABSTRACT

The glial fibrillary acidic protein, GFAP, forms the intermediate cytoskeleton in cells of the glial lineage. Besides the common GFAPα transcript, the GFAPε and GFAPκ transcripts are generated by alternative mRNA 3′-end processing. Here we use a GFAP minigene to characterize molecular mechanisms participating in alternative GFAP expression. Usage of a polyadenylation signal within the alternatively spliced exon 7a is essential to generate the GFAPκ and GFAPκ transcripts. The GFAPκ mRNA is distinct from GFAPε mRNA given that it also includes intron 7a. Polyadenylation at the exon 7a site is stimulated by the upstream splice site. Moreover, exon 7a splice enhancer motifs supported both exon 7a splicing and polyadenylation. SR proteins increased the usage of the exon 7a polyadenylation signal but not the exon 7a splicing, whereas the polypyrimidine tract binding (PTB) protein enhanced both exon 7a polyadenylation and exon 7a splicing. Finally, increasing transcription by the VP16 trans-activator did not affect the frequency of use of the exon 7a polyadenylation signal whereas the exon 7a splicing frequency was decreased. Our data suggest a model with the selection of the exon 7a polyadenylation site being the essential and primary event for regulating GFAP alternative processing.

INTRODUCTION

The Glial Fibrillary Acidic Protein (GFAP) gene is located on the human chromosome 17 (17q21), spanning 10 kb, and consisting of 9 exons. The corresponding GFAP protein is the principal intermediary cytoskeletal filament in mature astrocytes of the central nervous system (1). All intermediate filaments share a structure consisting of a conserved α-helical rod-like middle domain flanked by non-helical head and tail domains (2,3). Several isoforms of GFAP mRNA have been identified in mammals. Compared to the common form of GFAP, GFAPα, the mouse GFAPβ and GFAPγ isoforms (4) are produced by using different transcriptional start sites. The GFAPδ mRNA identified in the rat is the result of an alternative splicing event in intron 7 including the last 1255 nt of intron 7 fused to exon 8 (5). Finally, the GFAPε isoform found in humans is produced by the removal of an alternative exon 7a embedded in intron 7 (6). Importantly, this exon 7a contains an intrinsic polyadenylation signal. The GFAPε protein has a C-terminal sequence similar to GFAPδ (6). The GFAPε C-terminus specifically binds to the transmembrane proteins presenilin 1 and 2 (6). Furthermore, GFAPε cannot form homodimers, as can GFAPα, but it is capable of forming heterodimers with GFAPα and in this way to be integrated into intermediate filaments (7). The relative amounts of the two protein isoforms appear to directly influence the stability of the intermediate filaments (7,8). The GFAPε isoform is expressed most prominently in astrocytes of the subventricular zone of the brain, which is the principal source of neural stem cells in the adult human brain. GFAPε could be an important marker of neuronal stem cells and influence their functions (8). Recently, another GFAP mRNA isoform, GFAPκ, was identified in humans (9). The GFAPκ mRNA is produced by including intron 7 sequences and polyadenylation in exon 7a. The open reading frame of GFAPκ contains a stop codon in the included intron 7 sequences, and thus the GFAPκ protein differs from GFAPα in the C-terminal. Also, the relative amounts of the GFAPα and GFAPκ proteins appear to directly influence the stability of intermediate filaments. The mRNA ratio of GFAPκ/GFAPε is decreased during cortex development and increased in glioblastoma tumours, which indicates that the

*To whom correspondence should be addressed. Tel: +45 89421690; Fax: +45 86123173; Email: aln@humgen.au.dk

expression ratio could be a marker for the degree of glial cell differentiation (9).

Alternative usage of splicing and polyadenylation sequences frequently occurs in mammalian genes (10,11). Seventy-four percent of human multi-exon genes are estimated to be alternatively spliced (12), and the presence of two or more alternatively used poly(A) signals is estimated to occur in 49% of human genes (13). Regulation of alternative splicing and polyadenylation is controlled by sequences in the pre-mRNA (*cis*-elements) and interacting *trans*-factors (RNA or protein). Essential factors for splicing are the 5′-exon–intron splice site marked by the consensus sequence AG*GURAGU (* = splice site, R = purine), the 3′-splice site NYAG*R (Y = pyrimidine, N = purine or pyrimidine) preceded by a pyrimidine-rich stretch and the branch point sequence CURAY upstream of the 3′-splice site (14,15). Polyadenylation involves cleavage of the pre-mRNA and subsequent addition of 200–300 adenosine residues (16). *Cis*-elements in the pre-mRNA direct the factors to the correct cleavage site. Important is a highly conserved hexanucleotide AAUAAA located at 11–23 nt upstream of the cleavage site, and a less conserved G/U-rich downstream element. The mammalian cleavage and polyadenylation machinery consists of the cleavage/polyadenylation specificity factor (CPSF), cleavage stimulation factor (CstF), symplekin, cleavage factor I and II_m (CF I_m and CF II_m), poly(A) polymerase (PAP), poly(A)-binding protein nuclear 1 (PABPN1) and the CTD of RNA polymerase II (15). One of the best-elucidated mechanisms of alternative poly(A) site selection comes from studies of the immunoglobulin M (Ig μ) pre-mRNA. During B-cell maturation to plasma B cells there is a switch from a membrane-bound (μm) Ig μ to a secreted-form (μs) due to competing splicing (μm) and polyadenylation at an early polyadenylation site (μs). The μm polyadenylation site has a stronger binding affinity to CstF-64 than the μs site, meaning that the μm site is favoured in the case of a limited CstF-64 amount (17,18). The level of CstF-64 is increased during B-cell maturation and the use of the proximal μs polyadenylation site is favoured instead (17,18).

There are several examples of how the regulation of splicing of the terminal intron is coupled to 3′-end processing. Mutations of either the pyrimidine tract or the 3′-splice site of the last intron decrease the polyadenylation, and mutation of the AAUAAA decreases the splicing efficiency *in vitro* (19–21). *In vivo*, sequences within the last intron facilitate 3′-end formation (22) and more specifically, the pyrimidine tract in the terminal intron of the human β-globin gene stimulates polyadenylation both *in vitro* and *in vivo* (23). Several explanations of this coupling have been suggested. For example, poly(A) polymerase (PAP) interacts with $U2AF^{65}$ *in vitro* and stimulates the binding of $U2AF^{65}$ to a weak pyrimidine tract of a terminal intron (24), and $U2AF^{65}$ also interacts with CF I_m and stimulates 3′-end cleavage and polyadenylation *in vitro* (25). Moreover, interactions between the U1 and U2 snRNPs and polyadenylation factors may contribute to the coupling of splicing and 3′-end formation; the U1A protein of the U1 snRNP interacts with CPSF160 (26), and the U2 snRNP to CPSF (27) and both events stimulate 3′-end formation *in vitro*.

In addition to alternative splicing and polyadenylation signal selection regulation through mRNA stability is also involved in the control of cellular mRNA levels (28). For example in activated B cells, the stability of the μm mRNA is increased compared to the stability in resting cells equalling the stability of the μs mRNA (29). Thus, besides alternative splicing and polyadenylation mRNA stability also participates in the regulation of μm mRNA. mRNA *cis*-sequences and the length of the poly(A) tail are important determinants for the control of stability (30).

In this study, we have investigated the interplay between alternative splicing and polyadenylation of the GFAP pre-mRNA, which serves to generate the three isoforms of GFAP: GFAPα, GFAPε and GFAPκ. We find an intimate coupling between GFAP transcriptional activity, alternative splicing and polyadenylation.

MATERIALS AND METHODS

Sequences of primers and siRNAs are available as Supplementary Table S1.

Construction of minigenes

The GFAP wt minigene was constructed by inserting nucleotides 4677–10143 of the GFAP gene into the pTAG4 expression vector. DNA extracted from a Caucasian male was used as template in the PCR reactions. The GFAP-part of the construct was made in two parts and afterwards ligated together. The first part was generated using *Taq* DNA Polymerase (Amersham Biosciences), forward primer hsGFAP4677f (number included in the primer names indicate position in the GFAP gene sequence GeneID 2670 in GeneBank) carrying EcoRI site in the 5′-end, and reverse primer GFAP6061r carrying BglII site at the 5′-end. PCR conditions: 95°C 30 s, 60°C 30 s, 72°C 3 min; 35 cycles. The second part was made using Phusion High Fidelity DNA polymerase (Finnzymes), forward primer hsGFAP6062f with a BglII site at the 5′-end, and reverse primer hsGFAP10143r placed 290 bp downstream of the poly(A) site in exon 9 with a NotI site at the 5′-end. PCR conditions: 98°C 10 s, 71°C 30 s, 72°C 40 s; 30 cycles. The two GFAP-parts were inserted one at a time into the pTAG4 expression vector and verified by sequencing.

The GFAP + 1828 bp minigene was constructed by adding 1828 bp representing genomic sequences located downstream to the GFAP gene sequence present in the GFAP wt minigene. Forward primer was hsGFAP10144f and reverse hsGFAP11971r both carrying NotI sites, and Phusion High Fidelity DNA polymerase. PCR conditions: 98°C 10 s, 71°C 30 s, 72°C 30 s; 34 cycles.

The minigenes carrying other promoters than the SV40 promoter were constructed from the GFAP wt minigene. The SV40 promoter and its enhancer sequences were removed from the GFAP wt minigene and an AscI site added by site directed mutagenesis

(described subsequently). Forward primer pTAG4-delSV40f and reverse pTAG4delSV40r.

The β-globin and the tk promoters were amplified by PCR, by forward primer promoterf, reverse CATr, and using *Taq* DNA Polymerase. PCR conditions: 95°C 30 s, 60°C 30 s, 72°C 3 min; 30 cycles.

The GFAP promoter sequence including 2177 bp upstream of the start codon until 76 bp downstream of the start codon was amplified from human genomic DNA by PCR using Phusion High Fidelity DNA polymerase. Primers were GFAP-2177f and GFAP + 76r. PCR conditions: 98°C 10 s, 71°C 30 s, 72°C 1 min; 30 cycles. The SR protein expressing vectors were gifts (see Acknowledgments section) and the VP16 plasmid described before (31).

Site-directed mutagenesis

An overview of the mutations in the minigenes is available in Supplementary Figure S1. The mutated minigenes were made by site-directed mutagenesis. All reactions with plasmids <10 kb were performed under conditions: 2.5 U *PfuTurbo* DNA Polymerase (Stratagene), 10 pmol of each primer, 10 nmol dNTP, 5 µl 10× Reaction Buffer (Stratagene), 20 ng template and ddH_2O to a total volume of 50 µl. Cycle conditions: (80°C 5 min 95°C 30 s), 95°C 30 s, 50°C 1 min, 68°C 18 min; 20 cycles. All reactions with plasmids >10 kb were performed under conditions: 5 U *PfuTurbo* DNA Polymerase, 10 pmol of each primer, 20 nmol dNTP, 5 µl 10× Reaction Buffer, 20 ng template and ddH_2O to a total volume of 50 µl. Cycle conditions: (92°C 2 min), 92°C 10 s, 55°C 30 s, 68°C 24 min; 20 cycles.

Mammalian cell lines and transfections

Normal Human Astrocytes (NHA cells) from Cambrex was cultured in Astrocyte Basal Medium (Cambrex) added AGM SingleQuots (Cambrex). Other cell lines were cultured in D-MEM growth media (GIBCO) containing 10% heat-treated fetal calf serum, penicillin (1.2 g/l) and streptomycin (2.0 g/l) in 75 cm^2 flasks. Twenty-four hours before transfection cells were seeded into 6-well plates. Transfections were conducted with 1 µg DNA using FuGene 6 Transfection Reagent (Roche). Co-transfections of the GFAP wt minigene and the SR protein encoding plasmids were performed with 1 µg of each, and co-transfections of the GFAP wt minigene and VP16 were conducted with 1 µg GFAP minigene and 0.1 µg VP16 plasmid.

N2A cells were highly reproducible transfected and for this cause used in most of the experimental examinations. A172 and the primary astrocyte cells express endogenous GFAP and were used in experiments addressing the importance of regulatory mutants and *trans*-factors also in more biological relevant cellular systems. We note a day-to-day variation of the GFAP transcript ratios, and in the E7pA/E9pA ratio, in the order of 2-fold which could be caused by different cellular conditions.

Chemical treatments of cells

Actinomycin D (10 µg/ml), BAPTA (100 µM) and $CdCl_2$ (100 µM) (all from Sigma) treatment was started 48 h post transfection, heat-shock of cells was started 24 h post transfection, and after the indicated periods of time cells were harvested in Tri Reagent (Sigma) and frozen in –80°C before extraction of RNA.

RNA extraction and cDNA synthesis

Forty-eight hours post transfection total RNA was extracted using Tri Reagent and stored at −80°C. cDNA was synthesized from 1 g total RNA in 20 l reactions using iScript™ cDNA synthesis Kit (Biorad). After synthesis, the cDNA was diluted five times with double-distilled water and stored at 4°C.

Quantitative real-time PCR

Quantitative real-time PCR was performed on an iCycler Thermal Cycler (Bio-Rad) using the iCycler iQ™ Real-time PCR Detection System (Bio-Rad). All reactions were performed in triplicates in a total volume of 20 µl each using DyNAmoTM HS SYBR® GREEN qPCR Kit (Finnzymes). Two micro litres cDNA was used as template and 6 pmol of each primer (sequences in Table 1). Primer efficiency was measured by dilution standard curves (above 95%). The amount of mRNA was normalized to the measured expression of glyceraldehyde 3-phosphate dehydrogenase (GAPDH) mRNA in each sample and the quantification was done using the $2^{-\Delta\Delta C}{}_T$ method (32). For quantification of mRNA expression from the minigenes forward primer pTAG4E1E2 was used for GFAPα, GFAPε and GFAPκ, and reverse primers were hsGFAPE9r, hsGFAPE7Ar and hsGFAPI7r, respectively. For quantification of pig GFAP mRNA forward primer GFAPE6f was used for GFAPα, GFAPε and GFAPκ and reverse pigGFAPE9r, pigGFAPE7Ar and pigGFAPI7r, respectively. After each assay, the identity of the PCR products was confirmed by melting-curve analysis and gel electrophoresis.

Rapid amplification of cDNA 3′ ends (3′-RACE)

First-strand cDNA synthesis was synthesised from 3 µg total RNA using SuperScript™ II Reverse Transcriptase (Invitrogen) with 50 pmol of a modified oligo d(T) primer oligo(dT)V. RT–PCR was conducted using 5 µl cDNA, 5 U *Taq* DNA polymerase and 20 pmol of each primer. For the RT–PCR was used the reverse primer Oligo(dT)r tagging the oligo(dT)V primer and the forward primer pTAG4E1E2. PCR conditions: 95°C 30 s, 58°C 1 min, 72°C 3 min, 30 repeats. Nested PCR was conducted using 5 µl of the RT–PCR reaction as template under the conditions described above using reverse primer Oligo(dT)r and forward primer GFAP5242f. PCR products were separated with gel electrophoresis in 1% agarose, extracted and sequenced using DYEnamic ET terminator Cycle Sequencing Kit (Amersham Biotech Inc.).

RT–PCR

cDNA synthesized from A172 cells transiently transfected with either the GFAP wt, the GFAPΔ3′ss or GFAPmE7pA minigenes were used as template.

Forward primer pTAG4E1E2 were used for all GFAP isoforms and reverse primers hsGFAPE9r, hsGFAPE7Ar and hsGFAPI7r for GFAPα, GFAPε and GFAPκ, respectively. For possible reading trough of the poly(A) signal in exon 7a, primer GFAP6061r was used. As a positive control, 20 ng plasmid DNA was amplified by primers GFAP5242f and GFAP6061r. For PCR the Phusion High Fidelity DNA polymerase was used at the cycle conditions: 98°C 10 s, 71°C 30 s, 72°C 45 s; 36 cycles. PCR products were separated in a 1.2% agarose gel.

siRNA-mediated gene knockdown

Twenty-four hours before transfection, Hek293 cells were seeded into 6-well plates, at an amount of 1×10^5 cells per well. The cells were grown in RPMI growth medium (GIBCO) added 10% fetal calf serum, penicillin (1.2 g/l) and streptomycin (2.0 g/l), but during transfection cells were grown without antibiotics. Forty-five picomoles of siRNA (Dharmacon) was transfected into the cells using siLentFect (Biorad). Forty-eight hours after transfection the media was replaced with fresh medium, and 1 h after cells were transfected a second time, with either the GFAPmE7p(A) minigene alone or together with siRNA directed against Rrp6 or an irrelevant target as control, using Lipofectamine 2000 (Invitrogen). The cells were harvested after another 48 h. Five micrograms total RNA was treated with DNase (Turbo DNA-free kit, Ambion). cDNA was synthesized from 0.5 μg DNase treated RNA in 20 μ reactions using iScript™ cDNA synthesis Kit. After synthesis, the cDNA was diluted five times with double-distilled water and stored at 4°C. The RT–PCR was conducted as above, using identical primers, but the PCR only for 30 repeats.

Western blot

Forty-eight hours after the second transfection the medium was removed from the Hek293 cells and they were washed with PBS twice. The cells were scraped of the well in 1 ml PBS and aliquot into two eppendorf tubes, one for extraction of RNA and one for protein, and centrifuged 3 min at 1200 *g*. Cells were washed with PBS and centrifuged 10 s at 14 000 *g* and stored at –80°C. Cells were harvested in 200 μl lysis buffer (Tris–HCl 50 mM, EDTA 10 mM, SDS 1%) added one Complete Protease Inhibitor Cocktail tablet (Roche) by alternate freezing in dry ice and thawing in 37°C three times, incubated on ice for 30 min and centrifuged at 14 000*g* for 10 min. The supernatant was removed and the protein concentration was measured by Bradford. Four micrograms protein was added 5× Loading Buffer (Fermentas), 20× Reducing Agent (Fermentas) and PBS to a final volume of 15 μl and a 1× concentration, and the samples were heated to 100°C for 5 min. Western blotting analysis were performed at standard conditions and visualized by BM Chemiluminescence (Roche). The primary antibodies against Rrp6 (PM/Scl100, Ger Pruijn) and hnRNPC1/C2 (4F4 from Serafin Pinol-Roma) were diluted 1:4000 and 1:5000, respectively.

RESULTS

Establishment of a GFAP minigene

A map of the GFAP gene, the mRNA types and the corresponding proteins addressed in this study is shown in Figure 1A. GFAPα represents the most common isoform. GFAPε and GFAPδ are distinguishable only at the RNA level. To generate the GFAPε mRNA is used the exon 7a polyadenylation (E7pA) signal (6), whereas GFAPδ mRNA includes exon 7d, exon 8 and exon 9 (5). GFAPκ mRNA is generated in the absence of intron 7a splicing and simultaneous use of the E7pA signal. A putative novel GFAP mRNA, GFAPϕ, was deduced and generated when intron 7a splicing and E7pA signal use were absent. The expression pattern of the GFAPα, GFAPε and GFAPκ mRNAs has previously been described in brain samples and derived cell cultures (9).

To characterize the splicing events involved in alternative 3′-end formation of GFAP mRNA, we created a minigene including the 3′-part of the human GFAP gene inserted into the pTAG4 expression vector. GFAP sequences from intron 6 to position 291 after the exon 9 polyadenylation (E9pA) signal were fused to exons 1 and 2 from the human adenovirus 2 under control of the SV40 enhancer and promoter region (Figure 1B). The GFAP minigene was transfected into several different cell lines, and cDNA was examined for the presence of various GFAP mRNAs. GFAPα, GFAPε and GFAPκ mRNA were readily detectable whereas GFAPδ and GFAPϕ mRNA were undetectable (Figure 1C and data not shown). Other types of putative GFAP mRNAs were not detected (data not shown). Accordingly, the types of GFAP mRNAs expressed from the GFAP minigene resemble what was previously observed for endogenous GFAP in brain samples and derived cell cultures (9).

For a precise determination of the ratio between the three types of detectable GFAP mRNAs expressed from the minigene we performed a quantitative real-time RT–PCR analysis. A common forward primer was used together with reverse primers detecting each of the three examined GFAP mRNA types with resulting RT–PCR products in the size of 200 bp. The reverse primer for GFAPα mRNA detection is located in exon 9, the primer for GFAPε mRNA detection in exon 7a and the primer for GFAPκ mRNA detection in intron 7a which is included as an exon in the GFAPκ transcript. The RT–PCR assays were designed to span intron sequences to eliminate the contribution of contaminating DNA. Note that since the GFAPκ mRNA is 354 bp longer than the GFAPε mRNA, due to the inclusion of the intron 7a sequence in GFAPκ, the PCR reactions used for detecting GFAPε mRNA would in principle also detect GFAPκ mRNA. To eliminate this possibility the assay was run with a PCR extension time not allowing co-amplification of mRNA representing GFAPκ. The specificity of each PCR reaction for amplification of only one type of GFAP mRNA was verified by melting curve analysis and gel electrophoresis of the PCR products after each reaction (data not shown). Data is presented as expressed mRNA ratios since such values were

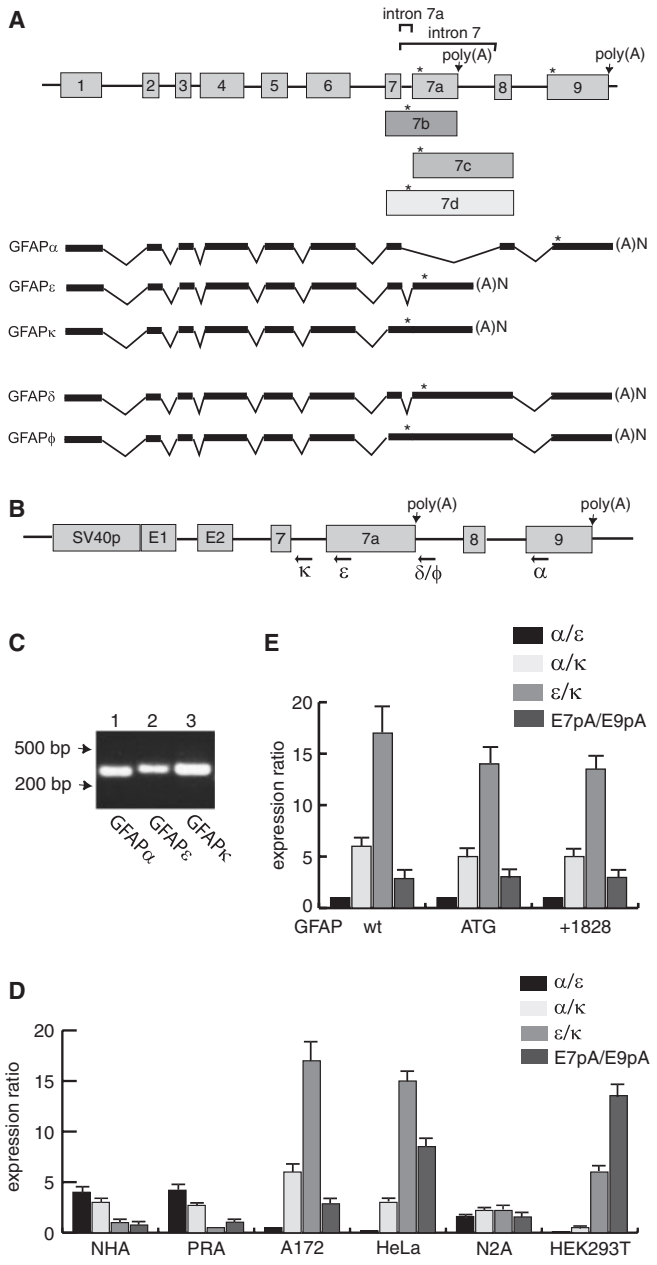

Figure 1. Construction and functional analysis of a GFAP minigene. (**A**) A schematic picture of the GFAP gene structure. The grey boxes denote the exons and the black horizontal lines the introns. Below is shown the arrangement of the exons in the GFAPα, GFAPε, GFAPκ, GFAPδ and GFAPΦ mRNA. The positions of stop codons are indicated by asterisks. (**B**) A schematic picture of the GFAP wt minigene. GFAP gene sequences from intron 6 through exon 9 were inserted into the pTAG4 vector. The vector contains the SV40 promoter and two internal exons (marked 1 and 2) and lacks internal poly(A) signals. The positions of the reverse primers used for real time PCR are denoted as black arrows: primers in intron 7a, exon 7a, intron 7 and exon 9 for amplification of GFAPκ, GFAPε, GFAPδ and GFAPΦ, and GFAPα, respectively. The forward PCR primer was spanning exon 1 and 2. (**C**) Gel electrophoresis of the PCR products from real-time PCR with the primers shown in (B). GFAPα (266 bp), GFAPε (299 bp) and GFAPκ (296 bp) are expressed from the GFAP wt minigene. Since the GFAPκ mRNA is 354 bp longer than the GFAPε mRNA, only GFAPε is amplified by the primer placed in exon 7a, at the used experimental conditions. (**D**) The expressed ratios of GFAPα/GFAPε, GFAPα/GFAPκ and GFAPε/GFAPκ mRNA in normal human astrocytes (NHA cells), primary rat astrocytes (PRA), A172, HeLa, N2A and HEK293T cells transiently transfected with the GFAP wt minigene. The SDs from three independent assays are shown. The E7pA/E9pA ratios are also shown. (**E**) The expressed ratios of GFAPα/GFAPε, GFAPα/GFAPκ and GFAPε/GFAPκ mRNA, as well as the E7pA/E9pA ratios, in A172 cells transiently transfected with the GFAP wt, the GFAP + ATG (coding) or the GFAP + 1828 bp minigenes. The E7pA/E9pA ratios are also shown.

more reproducible than the absolute expression levels, which varied experimentally. The GFAPε/GFAPκ mRNA ratio represents an estimate of exon 7a splicing efficiency. For a measure of the frequency of the two possible polyadenylation events possible for the GFAP transcripts we made the approximation that the ratio between transcripts terminating at the exon 7a polyadenylation signal and the exon 9 polyadenylation signal, E7pA/E9pA, was similar to the mRNA ratio (GFAPε + GFAPκ)/GFAPα. This is an acceptable approximation because GFAPα, GFAPε and GFAPκ were the only GFAP transcripts detectable from the minigene.

In transfected A172 human glioblastoma cells, GFAPα and GFAPε mRNAs were expressed to an equal ratio whereas GFAPκ mRNA was expressed at a 5- to 15-fold lower level (Figure 1D). Similar ratios of expression were observed in HeLa and HEK293T cells. In mouse N2A cells, the three GFAP mRNAs were expressed close to an equal level and in human NHA primary astrocytes and rat primary astrocytes GFAPα mRNA was expressed at the highest level (Figure 1D). Transfection titration experiments varying the concentration of the minigene in the transfections from 10 ng to 2 μg did not significantly influence the relative level of expression for the GFAP mRNAs (data not shown). We note a day-to-day variation, within a 2-fold range, of the GFAP transcript ratios and in the E7pA/E9PA ratio in the cellular transfection experiments presented.

In brain samples, endogenous GFAPα mRNA is expressed at a higher level than the GFAPε and GFAPκ mRNA (9). To examine if the GFAP minigene lacked the sequences required for enhancement of GFAPα mRNA expression we first examined the consequence of additional sequences after the polyadenylation sequence in exon 9. Inclusion of additional 1828 bp did not influence the expression ratio for the GFAP mRNAs (Figure 1E). We note that addition of this sequence extended the 3′-region of the GFAP gene to the position of the last exon of the neighbouring gene, coiled-coil domain containing 103, on chromosome 17 and may thereby include all intrinsic sequences required for GFAP E9pA signal usage.

The GFAP minigene contained no open reading frames. By site-directed mutagenesis we introduced a Kozak translational initiator sequence in exon 1. From this methionine an open reading frame extended into the GFAP part of the minigene in the frame normally used for the GFAP gene. The expression of the GFAPε C-terminal protein sequence from the GFAP-ATG minigene construct was verified by western blotting (data not shown). Introducing the open reading frame did not result in any significant variation of GFAP mRNA ratios (Figure 1E). We therefore conclude that translation

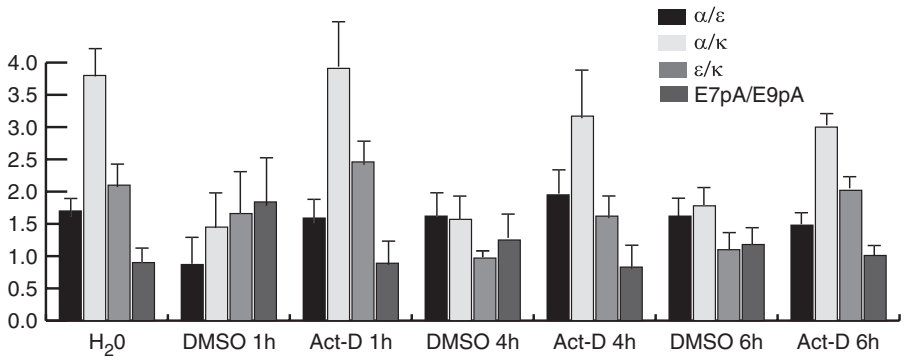

Figure 2. Determination of the relative GFAP mRNA stabilities. N2A cells transfected with the GFAP minigene were 48 h after transfection added actinomycin-D or as control the vehicle solution DMSO for the indicated time points. RNA was extracted and real-time RT–PCR was used to determine the ratios of GFAPα/GFAPε mRNA, GFAPα/GFAPκ mRNA and GFAPε/GFAPκ mRNA, as well as the E7pA/E9pA ratio. The labelling H_2O indicates transfected N2A cells not treated with DMSO and actinomycin-D.

is not severely affecting the ratio of the different GFAP mRNAs generated from the minigene.

The GFAP transcripts from the minigene were examined for their stability by a pulse-chase experiment as previously described (33). RNA polymerase II transcription was arrested by adding actinomycin-D to transfected N2A cells, and the amounts of GFAP mRNA present after 1, 4 and 6 h were measured by real-time PCR (Figure 2). Control cells were treated with the solvent of actinomycin-D, DMSO. Compared to the DMSO control the actinomycin-D treatment resulted in a 2-fold increase in the GFAPα/GFAPκ and GFAPε/GFAPκ mRNA ratios consistent with a preferential decrease in the amount of GFAPκ mRNA (Figure 2 and data not shown). However, if this decrease was due to an altered stability of the GFAPκ mRNA, the change in mRNA ratio would be expected to increase with time. This was not observed (Figure 2). We also noted that the GFAP mRNA ratios after actinomycin-D treatment resembled the profile normally present in N2A cells transfected with the GFAP minigene (Figure 2). Thus, the experiment indicates a similar mRNA stability for all three GFAP transcripts. The effect on the GFAPκ mRNA level seemed instead to be caused by the DMSO effect itself on the cells. We noted that treatment of the N2A cells with DMSO for longer timescales than the ones presented resulted not only in morphological cell changes but also in a decrease in the GFAPκ mRNA amounts in the actinomycin-D-treated cells (data not shown).

The cellular environment affects both the expression of the GFAP gene and the GFAP filament structure (1). Ca^{2+} is an example of a mediator for GFAP filament reorganization, and in addition Ca^{2+} levels can affect alternative splicing events. Accordingly, we considered whether the GFAP mRNA splicing and polyadenylation ratios could be affected by intracellular Ca^{2+} levels. By adding the cell permeable Ca^{2+} chelator BAPTA (34) a decrease in the GFAPα/GFAPε and GFAPα/GFAPκ ratios was observed together with an increase in the E7pA/E9pA ratio (Figure 3A). Thus, BAPTA treatment appears to affect the GFAP gene polyadenylation signal selection. We also addressed the importance of Ca^{2+} influx

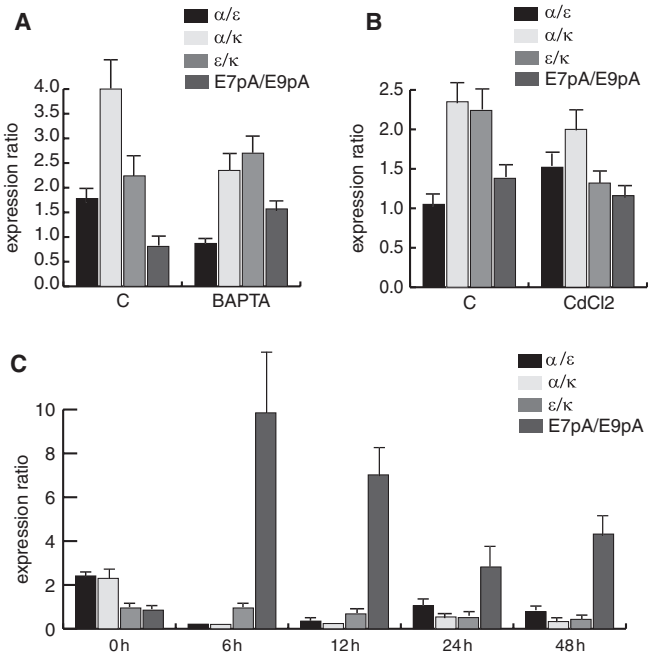

Figure 3. Environmental conditions affect GFAP polyadenylation signal selection. (**A**) N2A cells transfected with the GFAP minigene were added BAPTA or as control the vehicle solution $NaHCO_3$. RNA was extracted and real-time RT–PCR was used to determine the ratios of GFAPα/GFAPε mRNA, GFAPα/GFAPκ mRNA and GFAPε/GFAPκ mRNA, as well as the E7pA/E9pA ratio. (**B**) As in (A) except for the addition of $CdCl_2$ or as control H_2O. (**C**) Transfected N2A cells were 24 h after transfection incubated at 42°C for the indicated time points. RNA was analysed by real-time RT–PCR as described in (A).

by using Cd^{2+} to block the influx of extracellular Ca^{2+} through voltage dependent Ca^{2+} channels (34). No significant alteration in the ratio of polyadenylation signal selection was detected (Figure 3B).

Thermal stress is a physiological stress which may result in the turning on of heat shock response genes and reorganization of the cytoskeleton including GFAP filament reorganization. Altered GFAP expression is also observed after terminal stress. To further monitor the importance of terminal stress for the ratio of the

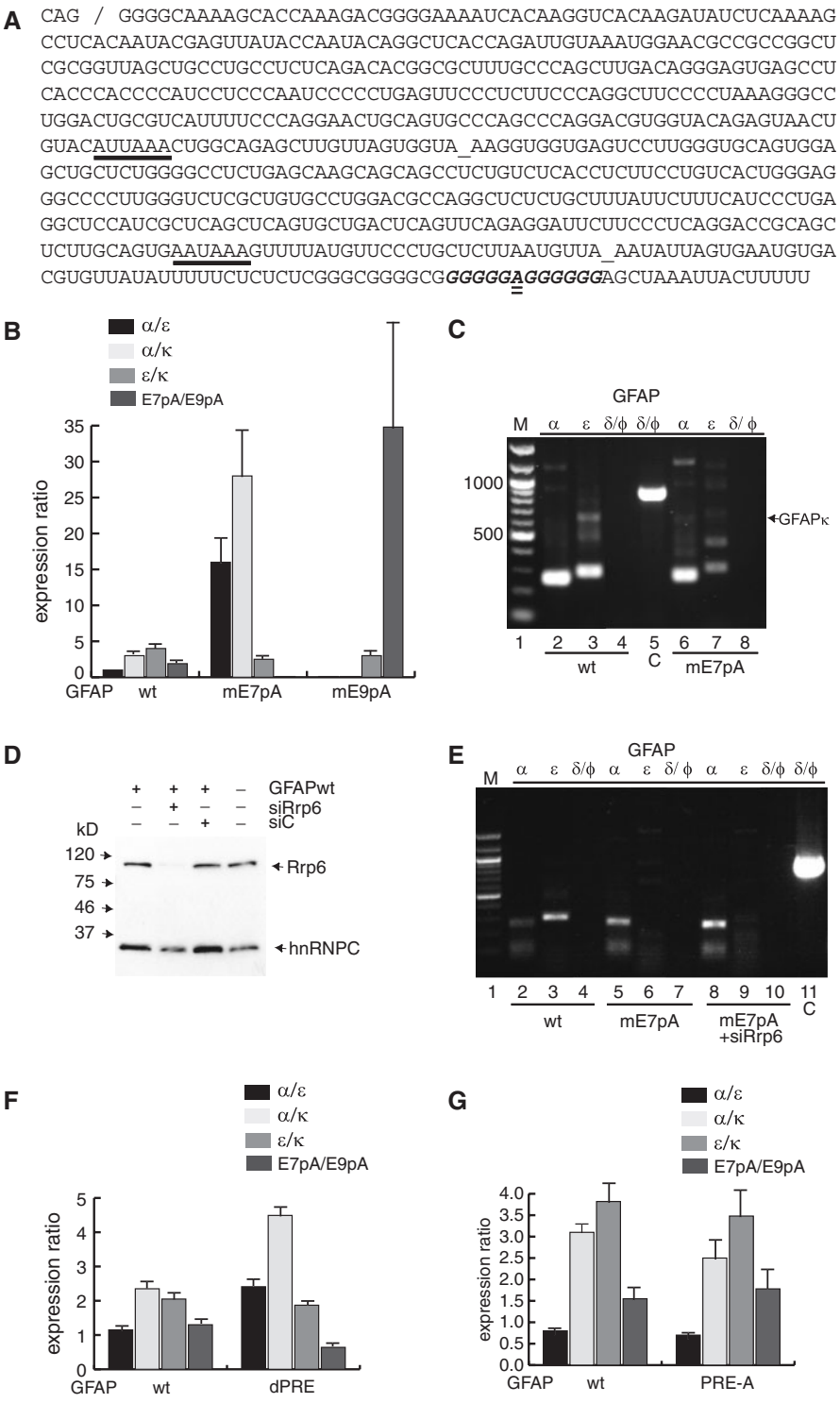

Figure 4. Exon 7a polyadenylation is required for alternative GFAP 3′-end processing. (**A**) The sequence of the polyadenylation signal in exon 7a with the AAUAAA hexamer and the AUUAAA hexamer (underlined). The position of poly(A) tail additions with origin from the polyadenylation signals were identified by 3′-RACE experiments and are marked with underscore. The G-rich region downstream the poly(A) signal compositing the PRE motif is shown in italic and bold. This region together with flanking sequences was deleted in the dPRE minigene. The position of the examined SNP is double underlined. The position of the intron 7a/exon 7a border is marked by a slash. (**B**) A172 cells were transiently transfected with the GFAP wt, GFAP-mE7pA (mutation of the exon 7a polyadenylation signal) or the GFAP-mE9pA (mutation of the exon 9 polyadenylation signal) minigenes. The expressed ratios were quantified by real-time PCR. (**C**) Gel electrophoresis of RT–PCR performed with cDNA made of total RNA extracted from A172 cells transiently transfected with either the GFAP wt minigene (wt) or GFAP-mE7pA. GFAPα (266 bp) and GFAPε (299 bp) are detected in (wt) and GFAP-mE7pA transfected cells. Note that the primers for GFAPε in this experimental setting also amplify cDNA representing GFAPκ (653 bp) (indicated by arrow). Neither GFAPδ nor GFAPΦ expression could be detected (expected sizes of 951 and 1305 bp, respectively). Plasmid DNA is used as a positive control for the reverse primer used for GFAPΦ amplification (lane C). The position of the reverse

GFAP transcripts we performed a 42°C heat-shock experiment using N2A cells transfected with the GFAP minigene. As observed for the BAPTA treatment the GFAPα/GFAPε and GFAPα/GFAPκ ratios decreased together with an increase in the E7pA/E9pA ratio (Figure 3C). Thus, also terminal stress seems to affect the selection of GFAP polyadenylation sites.

Characterization of the regulation of exon 7a polyadenylation signal selection

To address the function of alternative polyadenylation for GFAP 3′-end formation, we first analysed minigenes with mutations in the E7pA and E9pA signals (see legend to Figure 4A). Mutation of the E9pA signal decreased as expected both the absolute amount of GFAPα mRNA as well as its relative level to the other GFAP mRNAs (Figure 4B and data not shown). No effect was observed on the GFAPε/GFAPκ mRNA ratio. Mutation of the E7pA signal resulted in an increased amount of GFAPα mRNA, and only residual amounts of GFAPε and GFAPκ mRNA could be detected (Figure 4B and data not shown). This was also observed in primary human and rat astrocytes (data not shown). Due to the low level of both GFAPε and GFAPκ mRNA, calculations of expression ratios are connected with significant uncertainties but no gross alteration in the GFAPε/GFAPκ mRNA ratio was observed. Next, we addressed the molecular origin of the residual GFAPε mRNA and GFAPκ mRNA by 3′-RACE experiments. GFAPε and GFAPε mRNA expressed from the wt minigene were identified to be polyadenylated using the expected consensus polyadenylation signal AAUAAA. From the minigene with a mutation in the E7pA signal the GFAPε and GFAPκ mRNA bands represented cDNA polyadenylated by usage of another polyadenylation signal in exon 7a with weaker consensus AUUAAA (motif localization is shown in Figure 4A). Polyadenylation events originating from this new signal were observed only in the presence of the mutation within the E7pA signal. To further substantiate the observed dependence of exon 7a polyadenylation for generation of the GFAPε and GFAPκ mRNAs, we addressed the question if mutating the E7pA signal could result in inclusion of downstream sequences as new exonic sequences in the mRNA and thereby generate the GFAPδ or GFAPϕ mRNAs. RT–PCR analysis with reverse primers located downstream of the E7pA signal sequence revealed complete absence of cDNA representing GFAPδ or GFAPϕ (data not shown and Figure 4C). The lack of detectable GFAPδ or GFAPϕ mRNA could be a consequence of the cellular recognition of these mRNAs as aberrant. To address this possibility, we used RNAi to deplete cells for the mRNA degrading nuclear exosome component Rrp6 and examined GFAP mRNA expression from the normal minigene and the minigene with the E7pA signal mutation (Figure 4D and E). Rrp6 depletion resulted neither in the presence GFAPδ or GFAPϕ mRNAs nor in a significant increase of GFAPα, GFAPε or GFAPκ mRNA (Figure 4E and data not shown). Thus, the absence of mRNA including sequences downstream of the E7pA signal is most likely not explained by nuclear mRNA degradation but rather by splicing out of the entire intron 7. Together, these data indicate that usage of E7pA is essential for the quantitative generation of the GFAPε and GFAPκ mRNAs, and that absence of the functional E7pA signal does not produce GFAPδ or GFAPϕ mRNA. Accordingly, GFAP 3′-end alternative processing is dependent on a functional alternative polyadenylation site.

Given the regulatory importance of the E7pA site we searched for *cis*-sequences participating in this regulation. In the GFAP exon 7a, a G-rich sequence containing the motif, GGGGGGGGGGG, is located 90 bp downstream of the polyadenylation site. G-rich sequences have previously been shown to participate in enhancement of polyadenylation (35–37). The effect of deletion of this putative polyadenylation regulatory element (PRE) was examined in the context of the minigene. Complete PRE deletion resulted in a 2-fold increase in the GFAPα/GFAPε mRNA and GFAPα/GFAPκ mRNA ratios in primary rat astrocytes, and a corresponding decrease of the E7pA/E9pA ratio (Figure 4F). This effect was also observed in other cell lines (data not shown). Thus, the PRE is a candidate element for stimulation of E7pA usage. Interestingly, an SNP (A/G) at position 6 in the PRE motif (underlined above) is present in the human population. An A at position 6 in the PRE generates a MAZ protein-binding consensus, a site previously identified to be involved in RNA polymerase II pausing, transcriptional termination, and activation of polyadenylation (38–41). The frequency of the A and G alleles are 0.81 and 0.19, respectively, in the human Caucasian population (data not shown). The GFAP minigene used in our analysis has a G in the PRE, and by mutagenesis a minigene with A in the PRE was constructed. The effect of this change was analysed in a number of cell lines and no detectable alteration in the ratio between the different GFAP mRNAs was observed (Figure 4G and data not shown). We conclude that the PRE motif supports exon 7a polyadenylation independent of the PRE SNP sequence.

primers is schematically shown in Figure 1B. (**D**) Western blot of protein extracted from HEK293T cells transfected with either the GFAP-mE7pA minigene alone, or together with siRNAs against Rrp6 (siRrp6) or an unspecific siRNA (SiC) as control. To the left the marker sizes are shown. Expression of Rrp6 (100 kDa) is detected with a monoclonal antibody and as loading control the expression of hnRNPC1/C2 is shown (33 kDa). (**E**) RT–PCR of RNA extracted from the transfected HEK293T cells in (D). GFAPα and GFAPε and are detected as fragments of 266 and 299 bp, respectively. Neither GFAPδ nor GFAPΦ are detected (expected sizes of 951 bp and 1305 bp, respectively), in wt, GFAP-mE7pA, or GFAP-mE7pA and siRrp6 transfected cells. Plasmid DNA is used as a positive control for the reverse primer used for GFAPΦ amplification (lane C). The position of the reverse primers is schematically shown in Figure 1B. (**F**) *Cis*-elements influence alternative GFAP polyadenylation signal selection. Primary rat astrocytic cells were transiently transfected with either GFAP wt or GFAP-dPRE (deleted PRE sequence) minigenes. The expression ratios were quantified by real-time RT–PCR as previously described. (**G**) A minigene with nucleotide A in the SNP position 6 in the PRE motif was examined together with the wt minigene as in (F). Note the wt minigene contains a G nucleotide in the PRE SNP.

An inefficient 3′-splice site of intron 7a is a determinant of alternative GFAP 3′-end formation

We next addressed determinants for the regulation of the GFAP mRNA ratios. For these experiments, the N2A neuroblastoma cell line was used as we have observed highly reproducible transfection efficiency in this cell line. First, we examined the importance of the intron 7a 3′-splice site (for sequence see Figure 5A). A mutation within the splice site consensus CAG/G to ATT/T abolished, as expected, the generation of GFAPε mRNA (data not shown). Also the amount of transcripts terminated by the E7pA signal decreased indicating that the absence of the splice site, and thereby GFAPε mRNA production, did not result in a proportional increase in the amount of GFAPκ mRNA (Figure 5B). This further suggested a link between the use of the intron 7a 3′-splice site and the polyadenylation site. The GFAPα/GFAPκ mRNA ratio was increased to an expected degree if instead of GFAPε mRNA a proportional amount of GFAPα mRNA was generated (Figure 5B).

Alignment of the intron 7a 3′-splice site sequence with an optimal consensus splice site sequence revealed the presence of a putative optimal branch point sequence but also the presence of several purines within the sequence which is optimally composed of polypyrimidines (Figure 5A). A minigene was constructed with an optimal polypyrimidine tract, and expression analysis showed that

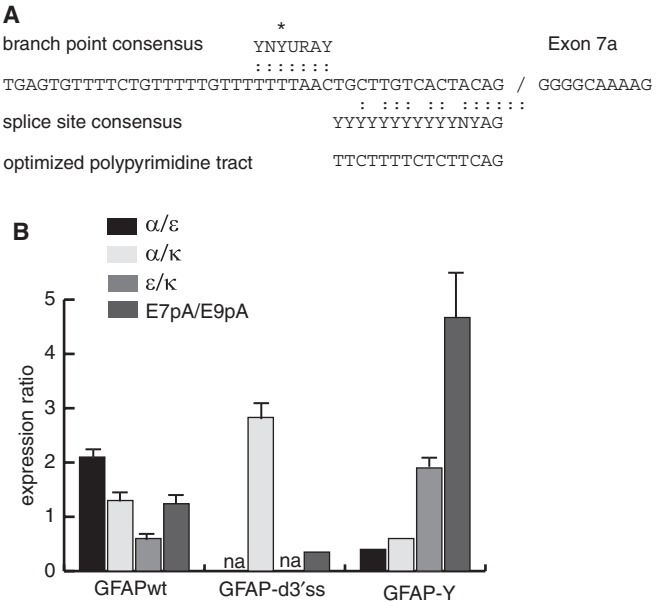

Figure 5. Exon 7a polyadenylation requires a functional 5′-splice site. (**A**) An overview of the pyrimidine tract preceding the 5′-splice site of exon 7a. The branch point consensus is shown to the left, and the consensus sequence of the 'ideal' pyrimidine tract is shown beneath the exon 7a sequence. Below, the sequence of the mutated, optimized sequence is shown. (**B**) The expressed ratios of GFAPα/GFAPε, GFAPα/GFAPκ and GFAPε/GFAPκ, together with the E7pA/E9pA ratio, in N2A cells transiently transfected with the GFAP wt, GFAP-d3'ss gene with a mutated intron 7a 3′-splice site, or the GFAP-Y minigene with an optimized polypyrimidine tract in the intron 7a 3′-splice site.

this mutation increases the amount of GFAPε mRNA both at the absolute level (data not shown) and relative to GFAPα and GFAPκ mRNAs (Figure 5B). The absolute amount of GFAPκ mRNA and the GFAPα/GFAPκ mRNA ratio did not decrease proportionally indicating that the total amount of mRNA generated from E7pA signal usage was increased (Figure 5B and data not shown). In accordance, the E7pA/E9pA ratio increased (Figure 5B). We note that even in the presence of the optimized polypyrimidine tract at the intron 7a 3′-splice site significant splicing from exon 7 to exon 8, which excludes exon 7a, does take place (Figure 5B). In conclusion, the composition of the GFAP intron 7a 3′-splice site is a limiting factor for exon 7a inclusion and polyadenylation, but clearly not the only determinant for transcriptional termination at the E7pA signal and exon 7a inclusion in the mature transcript. Even in the presence of an optimized intron 7a 3′-splice site, transcriptional read through of the E7pA signal and splicing out of the entire GFAP intron 7 was observed. This suggests that the recognition/utilization of the E7pA signal is also an important determinant for GFAP 3′-end formation.

Imperfect consensus splice sites are often supported by the presence of neighbouring splice-enhancing *cis*-sequences, and we searched for such sequences *in silico* by ESEfinder [(42) release 2.0 http://rulai.cshl.edu]. Within the first part of exon 7a three high-scoring putative splice enhancers (ESEs) were present (Figure 6A). All three ESE elements constituted putative SF2/ASF-binding sites. In addition, the ESE2 element is an SRp40-binding site and the ESE3 element an SRp40 and a SC35-binding site. Nucleotide substituting mutations were introduced in these sequences individually, and the effect on GFAP mRNA expression examined. In N2A cells, each of the mutations decreased the GFAPε/GFAPκ mRNA ratio indicating that all three ESE sequences possess splice enhancer activity (Figure 6B). Splice-enhancer activity was observed also in A172 cells, primary human astrocytes and primary rat astrocytes, but in these cell lines the effect of ESE2 was minimal (Figure 6C and data not shown). Introduction of a double mutation in ESE1 and ESE3 had no additive effect compared to the individual mutations (Figure 6B, 6C, and data not shown). In N2A cells, the ESE mutations have only a marginal effect on the E7pA/E9pA ratio (Figure 6B). In A172 cells, the ESE3 mutation resulted in a decreased E7pA/E9pA ratio supporting the fact that ESE sequences participate in E7pA signal selection (Figure 6C).

As the function of splice enhancers could be restricted to the presence of a weak 3′-splice sequence we examined the effect of the ESE1/ESE3 double mutant in combination with the optimized polypyrimidine tract at the 3′-splice site. Surprisingly, the ESE1/ESE3 double mutation completely abolished the gain mediated by the optimized polypyrimidine tract mutation for the GFAPε/GFAPκ mRNA ratios and E7pA/E9pA ratios (Figure 6D). Also, the decreased GFAPα/GFAPε mRNA ratio resulting from an optimized polypyrimidine tract was reverted by the combined mutation (Figure 6D), and, interestingly, the GFAPα/GFAPκ mRNA ratio increased (Figure 6D). This indicates that optimization of the

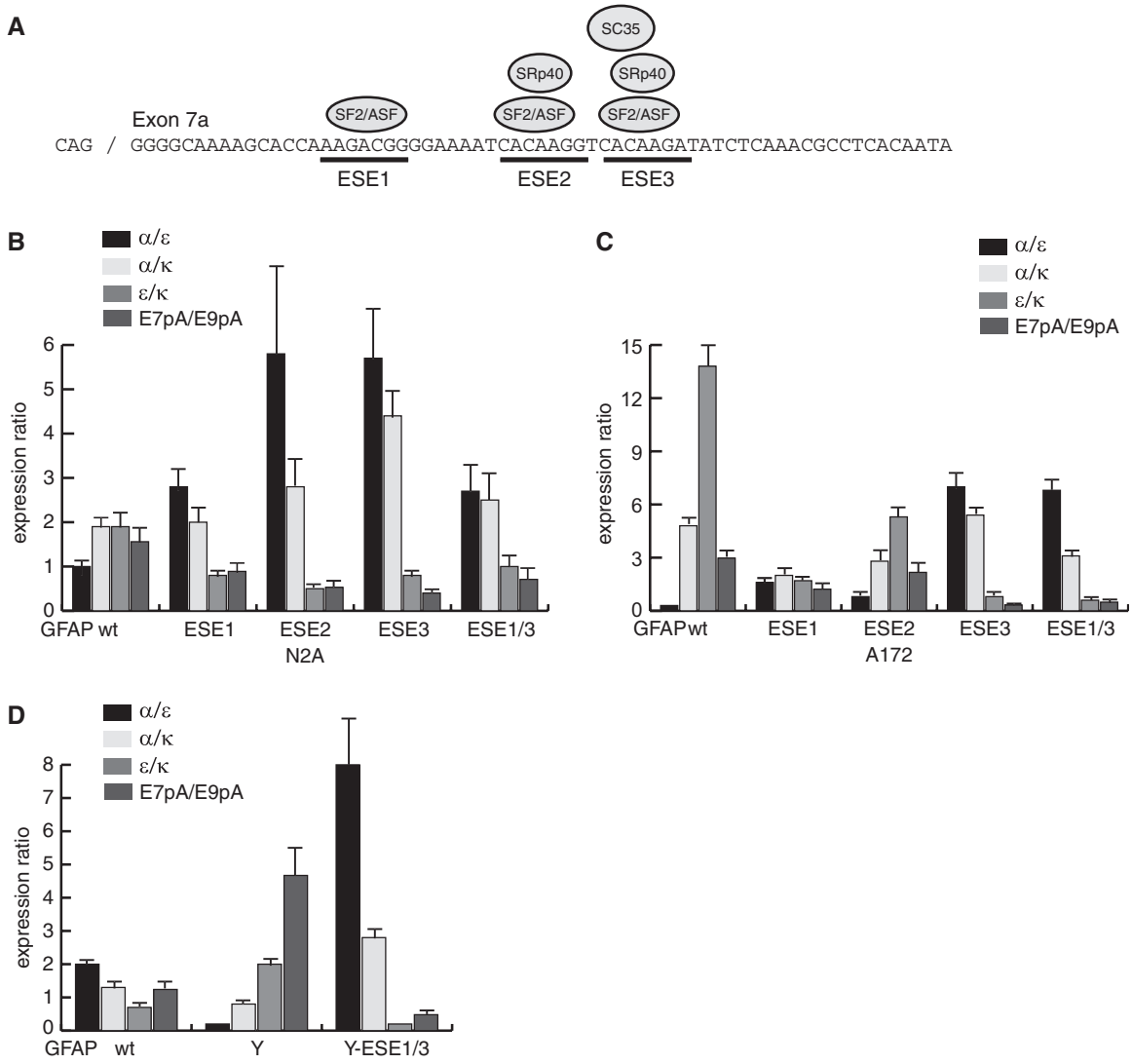

Figure 6. Exon 7a splicing and polyadenylation is regulated by SR proteins and exon splice enhancer, ESE, sequences. (**A**) The sequence of the 5′-part of exon 7a. The three putative ESEs are underlined. In order to test their functionality they were mutated either individually or in combination to produce the minigenes ESE1, ESE2, ESE3 and ESE1/3, respectively. (**B**) The expressed ratios of GFAPα/GFAPε, GFAPα/GFAPκ and GFAPε/GFAPκ, and the E7pA/E9pA ratio, in N2A cells transiently transfected with the GFAP wt or the ESE1, ESE2, ESE3 and ESE1/3 minigenes. (**C**) As (B) but with transfections in A172 cells. **(D)** The expressed ratios in N2A cells transiently transfected with the GFAP wt, GFAP-Y or the GFAP-Y-ESE1/3 combined mutation.

polypyrimidine tract alone is not sufficient, and still requires support from the ESE motifs to stimulate exon 7a inclusion and polyadenylation signal selection.

Overexpression of SR proteins stimulates alternative polyadenylation

Limitations of the amount of specific polyadenylation *trans*-factors have previously been shown to be important in the regulation of alternative polyadenylation signal selection. At first, we asked whether non-SR protein *trans*-factors, which in other regulatory systems influence polyadenylation signal selection, could also have an effect on GFAP E7pA selection. To this end, we cloned several of these factors and co-expressed them in A172 astrocytes together with the GFAP minigene. Expression of protein was verified by western blotting (data not shown). Note that such factors also have a potential to participate in the regulation of splicing. hnRNPH1, hnRNPF and CstF-64 had no effect on the ratio between the different GFAP mRNAs or on the absolute expression level of the individual mRNAs. PTB had a negative influence on the expression of GFAPα mRNA and accordingly resulted in decreased GFAPα/GFAPε and GFAPα/GFAPκ mRNA ratios and an increased E7pA/E9pA ratio (data not shown and Figure 7A). No significant alteration in the GFAPε/GFAPκ mRNA ratio was observed. Thus, PTB overexpression supports E7pA signal usage and a proportionally increased usage of the intron 7a 3′-splice site and accordingly proportional coupling of these events. Ectopic hnRNPH2 expression resulted in a relative increase in GFAPκ mRNA

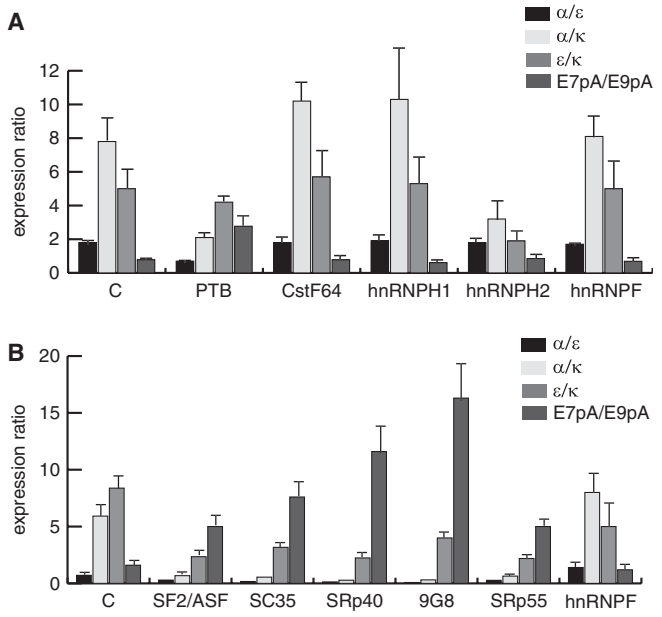

Figure 7. *Trans*-factors influence alternative GFAP polyadenylation signal selection. (**A**) Co-expression of the GFAP wt minigene and trans-factors involved in polyadenylation signal selection. A172 cells were transiently transfected with either the GFAP wt minigene and an empty vector or the GFAP wt minigene and a vector containing the open reading frame of factors determined to be involved in alternative polyadenylation. The GFAP mRNA ratios were quantified by real-time PCR. C indicates the control experiment in where the GFAPwt minigene was cotransfected with empty expression vector. (**B**) The GFAP mRNA ratios were determined in A172 cells transiently transfected with GFAP wt together with plasmids encoding the SR proteins ASF/SF2, SC35, Srp40, 9G8 or Srp55. C indicates the control experiment in where the GFAPwt minigene was cotransfected with empty expression vector. As a control RNA binding protein was included a transfection with an hnRNPF expression vector which in (A) was shown to have no effect on the expression ratios. The expressed ratios were quantified by real-time PCR.

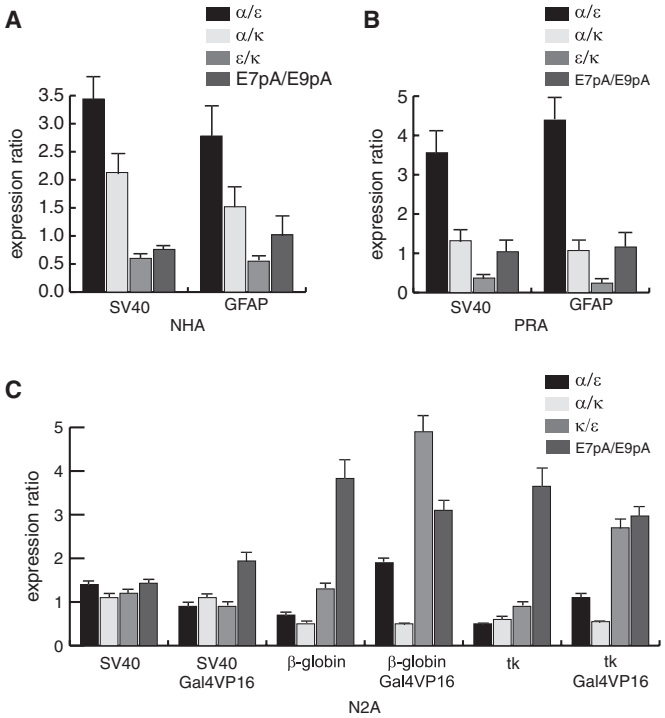

Figure 8. Promoter activity influences alternative GFAP 3′-end processing. (**A** and **B**) The SV40 promoter in the GFAP wt minigene was switched with the endogenous GFAP promoter and transiently transfected into NHA cells (A) or primary rat astrocytes (B). The indicated expressed ratios were quantified by real-time PCR. (**C**) The SV40 promoter in the GFAP wt minigene was switched with the β-globin minimal promoter or the tk minimal promoter with additional two upstream GAL4 recognition sites. The minigenes were transiently transfected into N2A cells co-transfected with the chimerical transcription factor GAL4-VP16. The expressed ratios were quantified by real-time PCR. Note that for illustration purposes the GFAPκ/GFAPε ratio is shown in this particular figure.

compared to the other two types of mRNA (Figure 7A). We have previously shown that the GFAPα/GFAPκ and GFAPε/GFAPκ mRNA ratios increased during cortex ageing (9). To examine if the expression pattern of PTB and hnRNPH2 followed the pattern of GFAP mRNA ratios we examined the expression level during cortex ageing. Both factors had a significantly altered expression at the examined time points but a correlation to GFAP mRNA expression patterns was not evident (data not shown).

We then examined how GFAP expression responded to co-transfection with expression vectors for different SR proteins. An increase in the amount of specifical GFAPκ mRNA was consistently observed in transfected A172 cells (Figure 7B and data not shown). The decrease in the GFAPε/GFAPκ mRNA ratio does not support that ectopic expression of SR protein stimulated the usage of the intron 7a 3′-splice site. By contrast, the E7pA/E9pA ratio was increased by SR protein overexpression (Figure 7B). This effect was not a general effect by overexpression of RNA-binding proteins as for example overexpression of hnRNPF not showed the same effect (Figure 7B). Titration analysis using from 10 ng to 1 μg of expression vector for SR protein resulted in the similar tendency for GFAP mRNA expression ratios (data not shown). Thus, SR protein overexpression stimulated E7pA signal selection, and this stimulation was not followed proportionally by intron 7a 3′-splice site usage.

Promoter activity influences GFAP 3′-end formation

Promoter controlled transcriptional initiation and elongation efficiency has previously been shown to influence the degree of alternative splicing (43,44). To address the importance of a specific promoter composition for the ratio between the different GFAP mRNAs we inserted the native GFAP promoter instead of the SV40 promoter in the context of the minigene. The GFAP promoter is specifically active in cells of astrocytic lineages. Comparison of the GFAP promoter minigene with the SV40 promoter minigene showed that the expression ratio between the different GFAP mRNAs was similar for the two constructs both in human and in rat primary astrocytes (Figure 8A and B and data not shown). We note that also the absolute expression levels of the GFAP mRNAs from the SV40 promoter and GFAP promoter minigenes were similar (data not shown). Introduction of

a selected set of the previously characterized mutations within the background of the GFAP promoter minigene also showed similar results as observed for the SV40 promoter driven minigene (data not shown).

To further monitor the importance of transcriptional activity for GFAP 3′-end formation we generated a series of minigenes under control of promoters inducible by the chimerical GAL4-VP16 transcription factor. Two GAL4-binding sites were introduced in either the β-globin or the thymidine kinase (tk) gene promoters in context of the minigene. The GFAP E7pA/E9pA ratios were different from the tk and β-globin promoter controlled minigenes as compared to the SV40 promoter controlled minigene indicating that different promoters may influence polyadenylation signal selection ratio (Figure 8C). We noted that the tk and β-globin minigenes had less basal promoter activity than for the SV40 minigene as the absolute GFAP mRNA expression levels were 10–15-fold lower (data not shown). GAL4-VP16 was previously shown to regulate alternative splicing by stimulating both transcriptional initiation and elongation (43,45,46). The minigene under control of the SV40 promoter was not affected by GAL4-VP16 co-expression as expected from the lack of GAL4 recognition motifs within the promoter. For the minigene under control of the β-globin promoter and two GAL4 recognition motifs GAL4-VP16 increased the absolute amount of GFAPα mRNA ~8-fold and for the tk promoter minigene 15-fold (data not shown). All three GFAP mRNAs had increased expression in response to GAL4-VP16 but the increase in GFAPε mRNA was less pronounced (Figure 8C and data not shown). Accordingly, the ratio between the different GFAP mRNAs was altered by GAL4-VP16 (Figure 8C). For both minigenes the GFAPα/GFAPε mRNA ratio was increased, the GFAPε/GFAPκ ratio was decreased, and the GFAPα/GFAPκ mRNA ratio was constant (Figure 8C). Notably, the E7pA/E9pA ratio was not altered significantly after induction with GAL4-VP16 (Figure 8C). In conclusion, E7pA signal selection seems to occur at the same frequency independent of the transcriptional rate, at least under the conditions examined, whereas the frequency of intron 7a 3′-splice site usage did not increase proportionally.

DISCUSSION

The occurrence of alternative C-termini of proteins may serve important functions and to achieve this, a complex scenario of regulatory events is required. Simple addition of a differentially used terminal exon is rarely possible due to 'nonsense mediated mRNA decay' [NMD, reviewed in (47)]. Regulation through nonsense mediated decay implies that the stop codon must be located within the ultimate or at the end of the penultimate exon; otherwise the mRNA will be subjected to degradation. Generation of a new C-terminal end of a protein by skipping of two or more terminal exons will therefore require the use of an alternative polyadenylation site in combination with the new stop codon or a complex alternative splicing scenario. Two types of alternative polyadenylation events occur at a high frequency in the human genome: the inclusion of a composite terminal exon, which is an exon extended due to the lack of 3′-splice site usage and which contains an intrinsic polyadenylation signal; or inclusion of an alternatively used terminal exon with an intrinsic polyadenylation signal (48). The efficiency of the alternative polyadenylation and splice site skipping/usage determines the efficiency of alternative 3′-processing. Alternative GFAP 3′-end formation uses both of these alternative polyadenylation events. The GFAPε mRNA is generated through usage of the skipped terminal exon 7a and GFAPκ mRNA through inclusion of intron 7a and exon 7a as the composite terminal exon 7b.

To identify regulatory events controlling the GFAP 3′-end formation we constructed a GFAP minigene to mimic endogenous GFAP regulation and to map *cis*-elements and *trans*-factors involved in this regulation. The abundance of the derived GFAP transcripts was measured by real-time RT–PCR. A clear limitation in such analysis is that they provide only steady-state values of the mRNA amounts based on the dynamic balance between transcription, polyadenylation and mRNA degradation. In this line the mRNA stability for the minigene-derived transcripts was examined. We found no evidence of stability differences for the three different GFAP transcripts. Accordingly, mRNA stability differences cannot be linked to the use of one particular polyadenylation signal. We note that experiments arresting transcription in astrocyte cell cultures indicated an equal stability for the endogenous GFAP transcripts as well (data not shown). The RT–PCR analysis of the expression pattern of the various mRNAs showed that the GFAPα/GFAPϵ mRNA, GFAPα/GFAPκ mRNA and E9pA/E7pA ratios are lower than the ratios for endogenous GFAP mRNA observed in brain tissue and derived cell lines. This discrepancy was not dependent on the 3′-length of the construct or the lack of translation from the construct. We note the possible absence of putative regulatory elements located between exon 1 and exon 7 of the GFAP gene and which could have influence on the splicing and polyadenylation events. Another obvious possibility is the lack of the correct transcriptional environment. Stable integration of the GFAP minigene into the genome of N2A cells resulted in GFAP mRNA ratios comparable to the values determined from transient analysis (data not shown). Thus, the ratio differences between the endogenous and the minigene expressed GFAP mRNA cannot be assigned solely to effects from transient experiments. We note that the GFAP gene is one of the most highly transcribed gene in maturate astrocytes (49). In this line, it will be interesting to examine 3′-processing also in the transcriptional regulatory context of chromatin in cells of astrocytic lineages.

It has become evident that splicing and polyadenylation can be coupled events that occur cotranscriptionally (15,16). Usage of the native GFAP promoter or the SV40 promoter in cells of astrocytic lineages did not change the GFAP isoform ratios, and the effect of different mutations analysed in this report was similar in the context of these two different promoters (Figure 8 and data not shown). However, we note that minigenes

containing the weakly transcribed tk and β-globin promoters contain altered GFAP transcript ratios (Figure 8). VP16 stimulates both initiation of transcription and elongation processivity (45,50). A processive elongation will help RNA Polymerase II elongate past sites where it is prone to stall or pause (44,51). The use of promoters inducible by VP16 showed that the E7pA/E9pA ratio is constant after inducing processive elongation. It indicates that exon 7a poly(A) site selection functions independently of the processivity of RNA Polymerase II. Participants of this independence could be regulatory sequences around the E7pA signal. We identified a sequence situated downstream of the E7pA signal, the PRE, which is similar to a polyadenylation regulatory motif identified in other genes, and we showed that this sequence contributes to GFAP 3′-formation through support of the E7pA signal usage. Four other regions surrounding the E7pA sequence and conserved to the mouse GFAP exon 7a were similarly analysed but no effect on either splicing or polyadenylation was detected (data not shown). The increased ratio of polyadenylation from E7pA after transcriptional induction by VP16 was associated with a lower ratio of intron 7a 3′-splice site usage. This could be mechanistically explained by a limitation in the recruitment of splice factors. Of the different *trans*-factors examined only the PTB protein had a proportional effect on splicing and polyadenylation of exon 7a. Thus, ectopic PTB expression did neither resemble the effect achieved by optimizing the polypyrimidine tract in the intron 7a 3′-splice site, nor the effect achieved by SR protein overexpression.

By mutating the AAUAAA hexamer in exon 7a, the GFAPα/GFAPε, GFAPα/GFAPκ and E9pA/E7pA ratios were increased. If inclusion of exon 7a could still occur without an AAUAAA hexamer in exon 7a, an mRNA containing a large exon starting at the 3′-splice site of intron 7a or at the position of the 3′-splice site in intron 6 and ending at the 5′-splice site of intron 9 could be expected. No such transcripts continuing downstream of the poly(A) signal were detected. This was also observed after depleting cells for Rrp6 of the nuclear RNA exosome. Altogether, this shows that splicing at the 3′-splice site in intron 7a does not occur without a functional poly(A) signal in exon 7a. This is in accordance with previous *in vitro* studies where mutation of the AAUAAA hexamer depresses splicing of the last intron (20,21). Further studies are needed to determine whether this is a direct effect of splicing or rather a consequence of a competitive removal of the entire intron 7 in the absence of the E7pA.

The 3′-splice site of GFAP intron 7a is a weak splice site based on score matrice calculations (http://www.fruitfly.org/seq_tools/splice.html, (52)). This weakness can be attributed to the presence of an imperfect consensus polypyrimidine tract. To analyse if the function of the E7pA signal depends on a functional 3′-splice site in intron 7a, an RT–PCR analysis was performed using RNA expressed from a minigene without a 3′-splice site. As expected, no transcripts corresponding to GFAPε mRNA was observed. Furthermore, no transcripts continuing downstream of the poly(A) signal was detected while mRNA representing GFAPκ was present. Thus, the poly(A) signal is functional without the intron 7a 3′-splice site. Quantitative analysis revealed a marked reduction in transcripts polyadenylated at the E7pA when the exon 7a splice site is mutated. This reduction was larger than would be expected if it was a result of a conversion to GFAPα mRNA of the amount of GFAPκ mRNA normally expressed. A simple explanation could be that the intron 7a 3′-splice site supported the selection of the E7pA site and in the absence of this splice site other sequence motifs, as for example the 3′-splice site in intron 6, to some extent could still support the usage of E7pA. The interrupted polypyrimidine tract upstream of the intron 7a 3′-splice site might impair U2AF binding. Optimizing the polypyrimidine tract strengthened the splice site, and the expression of GFAPε mRNA was increased relative to GFAPκ mRNA. More surprisingly, the E7pA/E9pA ratio was increased pointing to a positive effect also on exon 7a polyadenylation when the pyrimidine tract was optimized. PAP interacts with U2AF *in vitro* and stimulates binding of U2AF to a weak pyrimidine tract of a terminal intron (24). The pyrimidine tract, and not the splice site in the terminal intron of the human β-globin gene, stimulates polyadenylation *in vitro* and *in vivo* (23). Similar interactions could account for the coupling of the 3′-splice site in GFAP intron 7a with the E7pA signal.

Three exon 7a ESEs were found to be involved in the regulation of the alternative GFAP 3′-processing. The contribution from ESE1 and ESE3 was cell type independent. An ESE1/ESE3 double mutant showed the same mRNA ratios as were observed for the individual ESE mutations, which suggests that the ESE1 and ESE3 are not functional at the same time. This is in accordance with observations by Hertel and Maniatis who found that even though alternatively spliced exons often have several regulatory *cis*-elements, there is always only one active at a time, the others serving as back-up if the specific SR protein is not present (53). The co-expression of the GFAP wt minigene and plasmids expressing different SR proteins with the potential of binding to these ESE elements resulted in a decrease of the GFAPε/GFAPκ mRNA ratio while the E7pA/E9pA ratio increased. These findings indicate that SR proteins could have an effect not only on the splicing of intron 7a but also on the E7pA signal selection. Furthermore, mutation of ESE elements in the presence of an optimized pyrimidine tract results in a decreased E7pA/E9pA ratio, which also could indicate that ESE *cis*-elements have a role in enhancing polyadenylation (Figure 6D). Previously, it was shown that the SR protein SRp20 facilitates the use of the poly(A) signal in exon 4 of the calcitonin/calcitonin gene-related peptide (CT/CGRP) pre-mRNA (25). Similar interactions could account for our observations that SR proteins and ESEs are positively involved in the selection of the E7pA signal. The increased E7pA usage mediated by the SR proteins was not proportionally coupled to an increase in exon 7a splicing. Either the examined factors not limiting factors in the splice reaction or their overexpression directly disturbs splice complex formation. We note however that

SR protein overexpression did not result in any negative effect on the other splicing events in the cells.

Together, the presented results support a model for the alternative GFAP 3′-end formation wherein the activity of the GFAP exon 7a polyadenylation signal, and not 3′-splice site usage, is the primary determinant for the fraction of GFAP transcripts terminated by exon 7a. Subsequently, these GFAP transcripts can be spliced using the intron 7a 3′-splice site. The efficiency of these events are tightly regulated, both individually and coupled, which results in a possibility to precisely modulate the level of the three GFAP isoforms. Terminal stress and Ca^{2+} levels are two examples of environmental conditions previously described to be of importance to the GFAP filament organization. The direct effect on the GFAP filament structure through for example GFAP phosphorylation and the filament association of heat-shock factors is evident. The effect on the relative ratio of the GFAP transcripts described here can be important as we note that the GFAP isoforms have different functional properties in relation to filament assembly. Opposite to GFAPα the GFAPε and GFAPκ isoforms have no intrinsic filament forming capacity. At low-expression ratios, the GFAPε and GFAPκ isoforms assemble into GFAP filaments but interfere at high-expression ratios with the GFAP intermediate filament structure. Further delineation of the factors and mechanisms determining the GFAP 3′-end processing will be important in the functional characterization of these important GFAP isoforms.

SUPPLEMENTARY DATA

Supplementary Data are available at NAR Online.

ACKNOWLEDGEMENTS

We gratefully acknowledge Marianne Johansen, Bettina Hansen and Christian Westberg for technical assistance, Zitta Nygaard for critical reading of the manuscript, Dr John Lambert for rat primary astrocytes, Dr James Stévenin for the 9G8 expression vector, and Dr Adrian Krainer for the SC35, Srp40, Srp55 and ASF/SF2 expression vectors. This project was supported by funding from The Danish Cancer Society, The Danish Medical Research Foundation, Fonden til Lægevidenskabens Fremme, Fonden til Neurologisk Forskning, Kong Christian d. X's Fond, The Lundbeck Foundation and The Novo Nordisk Foundation. J.B. is a recipient of a PhD Fellowship from The Faculty of Health Sciences, University of Aarhus, Denmark. Funding to pay the Open Access publication charges for this article was provided by The Novo Nordisk Foundation and The Faculty of Health Sciences, University of Aarhus, Denmark.

Conflict of interest statement. None declared.

REFERENCES

1. Eng,L.F., Ghirnikar,R.S. and Lee,Y.L. (2000) Glial fibrillary acidic protein: GFAP-thirty-one years (1969–2000). *Neurochem Res.*, **25**, 1439–1451.
2. Geisler,N. and Weber,K. (1982) The amino acid sequence of chicken muscle desmin provides a common structural model for intermediate filament proteins. *EMBO J*, **1**, 1649–1656.
3. Parry,D.A. and Steinert,P.M. (1992) Intermediate filament structure. *Curr. Opin. Cell. Biol.*, **4**, 94–98.
4. Zelenika,D., Grima,B., Brenner,M. and Pessac,B. (1995) A novel glial fibrillary acidic protein mRNA lacking exon 1. *Brain Res. Mol. Brain Res.*, **30**, 251–258.
5. Condorelli,D.F., Nicoletti,V.G., Barresi,V., Conticello,S.G., Caruso,A., Tendi,E.A. and Giuffrida Stella,A.M. (1999) Structural features of the rat GFAP gene and identification of a novel alternative transcript. *J. Neurosci. Res.*, **56**, 219–228.
6. Nielsen,A.L., Holm,I.E., Johansen,M., Bonven,B., Jorgensen,P. and Jorgensen,A.L. (2002) A new splice variant of glial fibrillary acidic protein, GFAP epsilon, interacts with the presenilin proteins. *J. Biol. Chem.*, **277**, 29983–29991.
7. Nielsen,A.L. and Jorgensen,A.L. (2004) Self-assembly of the cytoskeletal glial fibrillary acidic protein is inhibited by an isoform-specific C terminus. *J. Biol. Chem.*, **279**, 41537–41545.
8. Roelofs,R.F., Fischer,D.F., Houtman,S.H., Sluijs,J.A., Van Haren,W., Van Leeuwen,F.W. and Hol,E.M. (2005) Adult human subventricular, subgranular, and subpial zones contain astrocytes with a specialized intermediate filament cytoskeleton. *Glia*, **52**, 289–300.
9. Blechingberg,J., Holm,I.E., Nielsen,K.B., Jensen,T.H., Jorgensen,A.L. and Nielsen,A.L. (2007) Identification and characterization of GFAPkappa, a novel glial fibrillary acidic protein isoform. *Glia*, **55**, 497–507.
10. Stamm,S., Ben-Ari,S., Rafalska,I., Tang,Y., Zhang,Z., Toiber,D., Thanaraj,T.A. and Soreq,H. (2005) Function of alternative splicing. *Gene*, **344**, 1–20.
11. Black,D.L. (2003) Mechanisms of alternative pre-messenger RNA splicing. *Annu. Rev. Biochem.*, **72**, 291–336.
12. Johnson,J.M., Castle,J., Garrett-Engele,P., Kan,Z., Loerch,P.M., Armour,C.D., Santos,R., Schadt,E.E., Stoughton,R. *et al.* (2003) Genome-wide survey of human alternative pre-mRNA splicing with exon junction microarrays. *Science*, **302**, 2141–2144.
13. Yan,J. and Marr,T.G. (2005) Computational analysis of 3′-ends of ESTs shows four classes of alternative polyadenylation in human, mouse, and rat. *Genome Res.*, **15**, 369–375.
14. Shapiro,M.B. and Senapathy,P. (1987) RNA splice junctions of different classes of eukaryotes: sequence statistics and functional implications in gene expression. *Nucleic Acids Res.*, **15**, 7155–7174.
15. Proudfoot,N. (2004) New perspectives on connecting messenger RNA 3′ end formation to transcription. *Curr. Opin. Cell. Biol.*, **16**, 272–278.
16. Proudfoot,N.J., Furger,A. and Dye,M.J. (2002) Integrating mRNA processing with transcription. *Cell*, **108**, 501–512.
17. Takagaki,Y., Seipelt,R.L., Peterson,M.L. and Manley,J.L. (1996) The polyadenylation factor CstF-64 regulates alternative processing of IgM heavy chain pre-mRNA during B cell differentiation. *Cell*, **87**, 941–952.
18. Takagaki,Y. and Manley,J.L. (1998) Levels of polyadenylation factor CstF-64 control IgM heavy chain mRNA accumulation and other events associated with B cell differentiation. *Mol. Cell*, **2**, 761–771.
19. Cooke,C. and Alwine,J.C. (1996) The cap and the 3′ splice site similarly affect polyadenylation efficiency. *Mol. Cell. Biol.*, **16**, 2579–2584.
20. Cooke,C., Hans,H. and Alwine,J.C. (1999) Utilization of splicing elements and polyadenylation signal elements in the coupling of polyadenylation and last-intron removal. *Mol. Cell. Biol.*, **19**, 4971–4979.
21. Niwa,M. and Berget,S.M. (1991) Mutation of the AAUAAA polyadenylation signal depresses in vitro splicing of proximal but not distal introns. *Genes Dev.*, **5**, 2086–2095.
22. Nesic,D., Cheng,J. and Maquat,L.E. (1993) Sequences within the last intron function in RNA 3′-end formation in cultured cells. *Mol. Cell. Biol.*, **13**, 3359–3369.
23. Millevoi,S., Geraghty,F., Idowu,B., Tam,J.L., Antoniou,M. and Vagner,S. (2002) A novel function for the U2AF 65 splicing factor in promoting pre-mRNA 3′-end processing. *EMBO Rep.*, **3**, 869–874.

24. Vagner,S., Vagner,C. and Mattaj,I.W. (2000) The carboxyl terminus of vertebrate poly(A) polymerase interacts with U2AF 65 to couple 3′-end processing and splicing. *Genes Dev.*, **14**, 403–413.
25. Millevoi,S., Loulergue,C., Dettwiler,S., Karaa,S.Z., Keller,W., Antoniou,M. and Vagner,S. (2006) An interaction between U2AF 65 and CF I(m) links the splicing and 3′ end processing machineries. *EMBO J.*, **25**, 4854–4864.
26. Lutz,C.S., Murthy,K.G., Schek,N., O'Connor,J.P., Manley,J.L. and Alwine,J.C. (1996) Interaction between the U1 snRNP-A protein and the 160-kD subunit of cleavage-polyadenylation specificity factor increases polyadenylation efficiency in vitro. *Genes Dev.*, **10**, 325–337.
27. Kyburz,A., Friedlein,A., Langen,H. and Keller,W. (2006) Direct interactions between subunits of CPSF and the U2 snRNP contribute to the coupling of pre-mRNA 3′ end processing and splicing. *Mol. Cell*, **23**, 195–205.
28. Garneau,N.L., Wilusz,J. and Wilusz,C.J. (2007) The highways and byways of mRNA decay. *Nat. Rev. Mol. Cell. Biol.*, **8**, 113–126.
29. Reed,D.J., Hawley,J., Dang,T. and Yuan,D. (1994) Role of differential mRNA stability in the regulated expression of IgM and IgD. *J. Immunol.*, **152**, 5330–5336.
30. Mangus,D.A., Evans,M.C. and Jacobson,A. (2003) Poly(A)-binding proteins: multifunctional scaffolds for the post-transcriptional control of gene expression. *Genome Biol.*, **4**, 223.
31. Nielsen,A.L., Ortiz,J.A., You,J., Oulad-Abdelghani,M., Khechumian,R., Gansmuller,A., Chambon,P. and Losson,R. (1999) Interaction with members of the heterochromatin protein 1 (HP1) family and histone deacetylation are differentially involved in transcriptional silencing by members of the TIF1 family. *EMBO J.*, **18**, 6385–6395.
32. Livak,K.J. and Schmittgen,T.D. (2001) Analysis of relative gene expression data using real time quantitative PCR and the 2(-Delta Delta C(T)) Method. *Methods*, **25**, 402–408.
33. Vasilopoulos,Y., Cork,M.J., Teare,D., Marinou,I., Ward,S.J., Duff,G.W. and Tazi-Ahnini,R. (2007) A nonsynonymous substitution of cystatin A, a cysteine protease inhibitor of house dust mite protease, leads to decreased mRNA stability and shows a significant association with atopic dermatitis. *Allergy*, **62**, 514–519.
34. Rozic-Kotliroff,G. and Zisapel,N. (2007) Ca2+ -dependent splicing of neurexin IIalpha. *Biochem. Biophys. Res. Commun.*, **352**, 226–230.
35. Qian,Z.W. and Wilusz,J. (1991) An RNA-binding protein specifically interacts with a functionally important domain of the downstream element of the simian virus 40 late polyadenylation signal. *Mol. Cell. Biol.*, **11**, 5312–5320.
36. Dalziel,M., Nunes,N.M. and Furger,A. (2007) Two G-rich regulatory elements located adjacent to and 440 nucleotides downstream of the core poly(A) site of the intronless melanocortin receptor 1 gene are critical for efficient 3′ end processing. *Mol. Cell. Biol.*, **27**, 1568–1580.
37. Arhin,G.K., Boots,M., Bagga,P.S., Milcarek,C. and Wilusz,J. (2002) Downstream sequence elements with different affinities for the hnRNP H/H' protein influence the processing efficiency of mammalian polyadenylation signals. *Nucleic Acids Res.*, **30**, 1842–1850.
38. Yonaha,M. and Proudfoot,N.J. (2000) Transcriptional termination and coupled polyadenylation in vitro. *EMBO J.*, **19**, 3770–3777.
39. Ashfield,R., Enriquez-Harris,P. and Proudfoot,N.J. (1991) Transcriptional termination between the closely linked human complement genes C2 and factor B: common termination factor for C2 and c-myc? *EMBO J.*, **10**, 4197–4207.
40. Yonaha,M. and Proudfoot,N.J. (1999) Specific transcriptional pausing activates polyadenylation in a coupled in vitro system. *Mol. Cell*, **3**, 593–600.
41. Ashfield,R., Patel,A.J., Bossone,S.A., Brown,H., Campbell,R.D., Marcu,K.B. and Proudfoot,N.J. (1994) MAZ-dependent termination between closely spaced human complement genes. *EMBO J.*, **13**, 5656–5667.
42. Cartegni,L., Wang,J., Zhu,Z., Zhang,M.Q. and Krainer,A.R. (2003) ESEfinder: A web resource to identify exonic splicing enhancers. *Nucleic Acids Res.*, **31**, 3568–3571.
43. Kadener,S., Cramer,P., Nogues,G., Cazalla,D., de la Mata,M., Fededa,J.P., Werbajh,S.E., Srebrow,A. and Kornblihtt,A.R. (2001) Antagonistic effects of T-Ag and VP16 reveal a role for RNA pol II elongation on alternative splicing. *EMBO J.*, **20**, 5759–5768.
44. Kadener,S., Fededa,J.P., Rosbash,M. and Kornblihtt,A.R. (2002) Regulation of alternative splicing by a transcriptional enhancer through RNA pol II elongation. *Proc. Natl Acad. Sci. USA*, **99**, 8185–8190.
45. Blau,J., Xiao,H., McCracken,S., O'Hare,P., Greenblatt,J. and Bentley,D. (1996) Three functional classes of transcriptional activation domain. *Mol. Cell. Biol.*, **16**, 2044–2055.
46. Nogues,G., Kadener,S., Cramer,P., Bentley,D. and Kornblihtt,A.R. (2002) Transcriptional activators differ in their abilities to control alternative splicing. *J. Biol. Chem.*, **277**, 43110–43114.
47. Weischenfeldt,J., Lykke-Andersen,J. and Porse,B. (2005) Messenger RNA surveillance: neutralizing natural nonsense. *Curr. Biol.*, **15**, R559–R562.
48. Tian,B., Pan,Z. and Lee,J.Y. (2007) Widespread mRNA polyadenylation events in introns indicate dynamic interplay between polyadenylation and splicing. *Genome Res.*, **17**, 156–165.
49. Pekny,M. and Pekna,M. (2004) Astrocyte intermediate filaments in CNS pathologies and regeneration. *J. Pathol.*, **204**, 428–437.
50. Yankulov,K., Blau,J., Purton,T., Roberts,S. and Bentley,D.L. (1994) Transcriptional elongation by RNA polymerase II is stimulated by transactivators. *Cell*, **77**, 749–759.
51. Mason,P.B. and Struhl,K. (2005) Distinction and relationship between elongation rate and processivity of RNA polymerase II in vivo. *Mol. Cell*, **17**, 831–840.
52. Reese,M.G., Eeckman,F.H., Kulp,D. and Haussler,D. (1997) Improved splice site detection in Genie. *J. Comput. Biol.*, **4**, 311–323.
53. Hertel,K.J. and Maniatis,T. (1998) The function of multisite splicing enhancers. *Mol Cell*, **1**, 449–455.